



The crustal structure of Cuba derived from Receiver Function Analysis

Bladimir Moreno Toiran

Inst. of Solid Earth Physics, University of Bergen, Allegt. 41, 5007 Bergen, Norway; Centro Nacional de Investigaciones Sismológicas, Calle 17, No. 61 e/ 4 y 6 Vista Alegre, Santiago de Cuba, Cuba

Received 17 December 2001; accepted in revised form 10 December 2002

Key words: crustal Structure, Cuba, Moho depth, Receiver Function, velocity model

Abstract¹

Teleseismic waveforms recorded by the broadband seismic stations of Cuba have been analysed using the receiver function method. The thickness of the crust at seven sites on the island was found to be in agreement with previous studies. The results suggest a clear layering at some sites with a Moho depth ranging between 18 and 31 km. In eastern Cuba, the seismic stations located in the south experience thinner crust in comparison with stations located in the north, which is consistent with a southward gradual thinning revealed by other studies. The thickest crust is found at Cascorro (CCC) in the interior part of the island. The velocity models computed from the receiver-function inversion show an upper-mantle P-wave velocity between 7.6 and 8.0 km/sec. Low velocity zones are visible at some sites.

Introduction

The island of Cuba is situated in the Caribbean region within the Antilles island arc. It is located in the southern margin of the North America plate in direct contact with the Caribbean plate, where a mechanism of strike-slip deformation dominates. Previous investigators have identified two different active tectonic periods in the history of development of the crust in Cuba. During the first period (Jurassic-Middle Eocene), an island arc with continental crust was formed on oceanic basement (Pushcharovskiy, 1979). Subsequently (Late Eocene – Quaternary), the earlier-formed nappe-fold complexes, as a whole, were subjected to deformations of a fundamentally different character. They are expressed in rises and basins of the present topography, and consequently in the features of the facies and thicknesses of the Middle and Upper Cenozoic sediments (Makarov, 1986).

The geology of Cuba differs significantly from that of other areas of the Greater Antilles in several as-

pects. Cuba contains Precambrian rocks and extensive outcrops of continental margin, sedimentary rocks of Jurassic to Cretaceous age. It is structurally characterized by large thrust and nappe structures, which are not present in the other islands of the northern Caribbean (Draper and Barros, 1994). Over most of its length, Cuba is the dividing line between extremely stable geologic conditions to the north and a complex one to the south (Pardo, 1975). According to Pardo (1975), much of the north coast of Cuba belongs to the Florida-Bahama carbonate province. On the other hand, most of the southern part of the island consists of metamorphosed sedimentary and acidic igneous rocks. In between, as a result of the contact between the Bahamas platform and the Cuban island arc, there is a relatively narrow belt of extremely folded and faulted material with ultra-basic igneous rocks and many types of volcanics and volcanic-derived sediments.

Gravimetric data (Soloviev et al., 1964) shows that Western Cuba appears to be in local mass balance, to judge by negative Bouguer anomalies (–50 to +50 mGals). The gravity and refraction data of central Cuba are less determinate, but probably the crust is in mass balance there too (Case et al., 1990). Eastern Cuba exhibits very large positive Bouguer anomalies

¹Statement of exclusive submission: This paper has not been submitted elsewhere in identical or similar form, nor will it be during the first three months after its submission to *Journal of Seismology*.

(+100 to +150 mGals), even over some high elevations, and thus shows a large mass imbalance. The excess mass beneath eastern Cuba indicates a shallow fragment of upper mantle or oceanic crust, as shown by the many exposed mafic and ultramafic bodies (Case et al., 1990).

The characterization of the tectonics and structure of the crust presented in previous studies were mainly based on seismic refraction methods combined with gravimetric data, deep drilling and satellite photographs (Shcherbakova et al., 1977, 1978; Bovenko et al., 1980, 1982; Bush and Shcherbakova, 1986). The use of other crustal-study techniques became feasible with the installation of a new digital broadband seismic network in 1998 (Figure 1). The network records teleseismic earthquakes, which can be used for crustal studies with the receiver function method (Langston, 1979; Ammon, 1991). This technique has been widely used to define first-order discontinuities or transition zones below seismic stations. Our intention in this work is to provide new information of crustal thickness and shallow discontinuities at sites where no previous studies have been done as well as compare our results with those sites where different methods of crustal studies have been employed.

Previous studies of the crustal structure in Cuba

The crust of Cuba is rather complex, ranging from oceanic to continental type. According to Bush and Shcherbakova (1986), the Cuban region consists of a tectonic junction of three dissimilar crustal blocks: (1) an autochthonous segment of the North American plate with continental crust; (2) a Cretaceous volcanic island arc with transitional crust and overthrust structure; and (3) an autochthonous fragment of a Paleocene volcanic island arc. Otero et al. (1998), based on previous seismic profiles (Shcherbakova et al., 1977, 1978; Bovenko et al., 1980, 1982) and gravity data, classified these three blocks as a thick transitional crust, a thin transitional crust, and an oceanic crust (lower map in Figure 1). These previous studies suggest that the Moho surface seems to be affected by two fault systems. One system, trending southwest-northeast, such as Cauto-Nipe fault (CNF) and another longitudinal to the island, such as the fault system defining the 'axial fault' of Cuba (upper map in Figure 1).

Shcherbakova et al. (1977, 1978) defined a three-layer crust in western Cuba: an upper layer hav-

Table 1. Broadband seismic stations of Cuba

Station	Latitude North (°)	Longitude West (°)	Elevation (meters)
MAS	20.1760	74.2310	350
RCC	19.9953	75.6965	100
LMG	20.0673	77.0047	200
MOA	20.6583	74.9568	140
CCC	21.1937	77.4172	90
MCG	22.3333	80.0000	100
SOR	22.7830	83.0180	206

ing velocities of 2.0 to 4.6 km/sec, associated with volcanic metasedimentary and carbonate metaclastic formations; a middle layer having average velocities of 6.2 km/sec; and a lower crustal layer having average velocities of 7.2 km/sec. The crust ranges from 21 to 33 km in thickness. In eastern Cuba, Bovenko et al. (1980, 1982) recognized an upper layer having velocities of 4.0 to 5.8 km/sec and a second layer having velocities of 6.9 to 7.8 km/sec; a mantle velocity of 8.1 km/sec was assumed in their calculations. A great variation in crustal thickness, from about 12 to 34 km, was found in their study. The distribution of the seismic profiles across the country is shown in Figure 1.

Satellite photograph interpretation (Bush and Shcherbakova, 1986) has been used to refine the position of Cuba's 'axial fault', which extends over 800 km along the entire island (upper map in Figure 1). Bush and Shcherbakova (1986) interpreted this 'axial fault' as the southern boundary of the contact zone between the Cuban island arc and the Bahama platform. Based on joint interpretation of gravity and seismic refraction data, they found drastic changes in the crustal thickness across this obduction zone. The area of plate interaction is a fault zone dipping south at about 65°, 5–10 km wide and traceable to a depth of 55 km (Bush and Shcherbakova, 1986). This fault zone roughly represents a dividing line between a northern miogeosynclinal part and southern eugeosynclinal part of the island. Within the northern, miogeosynclinal segment of Cuba, the thickness of the continental crust fluctuates within the 27–35 km range (Bush and Shcherbakova, 1986). The crust is substantially different in the southern, eugeosynclinal part of Cuba. It is categorized as a transitional and oceanic crust (Otero et al., 1998). Another remarkable change of the crustal properties also occurs across CNF (Figure 1). Otero

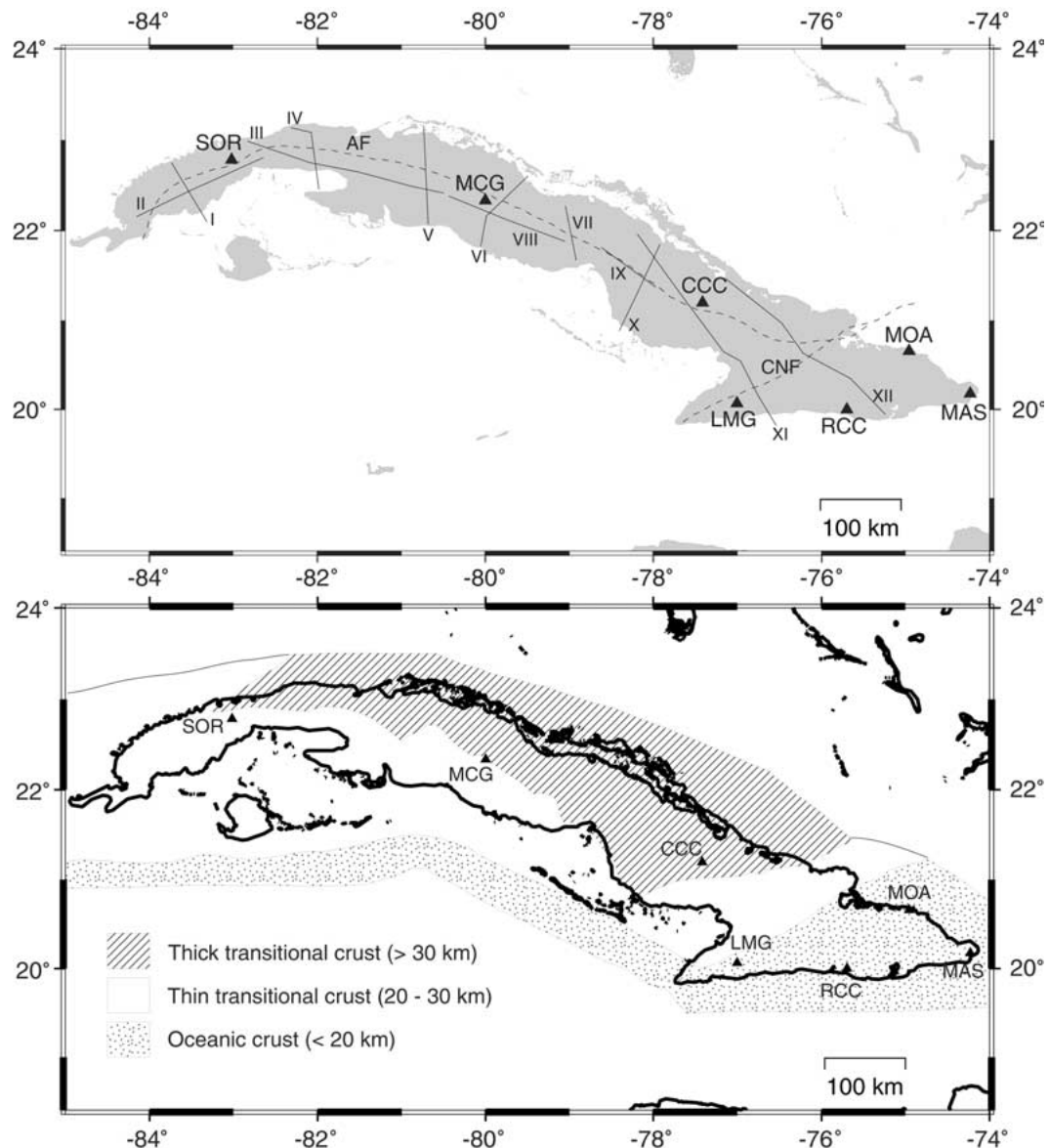


Figure 1. Upper map: Location of seismic stations and seismic cross sections in Cuba. The references of the profiles are: I, V – (Shcherbakova et al., 1977, 1978; Bush and Shcherbakova, 1986); II, III, IV, VI, VII, VIII – (Shcherbakova et al., 1977, 1978); XI – (Bovenko et al., 1980, 1982; Bush and Shcherbakova, 1986); IX, X, XII – (Bovenko et al., 1980, 1982). Dashed lines represent the ‘axial’ fault (AF) (contact zone between the Cuban island arc and the Bahamas platform) and the Cauto-Nipe fault (CNF). Lower map: Classification of the crust in Cuba according to Otero et al., 1998. Solid triangles represent the location of the Cuban seismic stations.

et al. (1998), presented this fault as a dividing line between transitional and oceanic crust.

Source of data

The seismic stations used in this study have 3-component broadband seismometers, which are op-

erating at a dynamic range of 96 db (Table 1 and Figure 1). They are recording at 100 samples per seconds in the 0.05 Hz to 40 Hz frequency band (Moreno, 2002). A total of 17 teleseismic events were selected from May 1998 to November 2000 at distances ranging between 37° and 80° (Figure 2 and Table 2). The preparation of data was done with the SAC software (Goldstein, 1999). The receiver func-

Table 2. List of earthquakes used in this study

No.	Date	Time	Longitude	Latitude	Depth	Magnitude (Ms)
1	19980522	0448	-64.96	-17.33	33	6.0
2	19980607	1610	-67.43	-31.28	113	5.7
3	19980729	0714	-71.08	-32.25	51	6.2
4	19980903	1737	-71.55	-29.29	33	6.5
5	19990320	1047	-177.87	51.72	33	7.0
6	19990801	1247	-176.31	51.68	62	5.6
7	19990801	1606	-117.07	37.39	5	5.6
8	19990822	0935	-74.82	-40.42	33	6.3
9	19991013	0133	-161.19	54.72	33	6.3
10	19991016	0946	-116.32	34.50	10	7.3
11	19991206	2312	-154.56	57.45	33	6.8
12	20000316	1519	-125.28	40.39	8	5.8
13	20000421	0435	-178.16	51.41	33	5.8
14	20000423	1701	-62.94	-28.38	609	6.2
15	20000512	1843	-66.45	-23.55	225	7.2
16	20000602	1113	-130.18	44.50	10	5.9
17	20000711	0132	-154.51	57.60	56	6.5

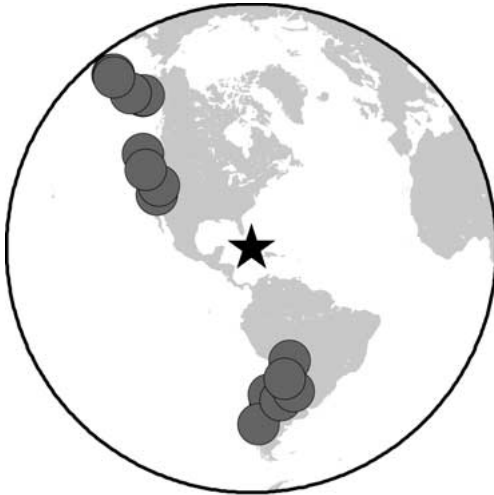


Figure 2. Location of the earthquakes used in this study.

tions computation and inversion were performed with the programs developed by Ammon et al. (1990).

Receiver Function Analysis, theory

Teleseismic P-waves that are incident upon the crustal section below a seismic station produce P to S conversions at crustal boundaries as well as multiple reverberations in the shallow layers. The P to S conversion

has much stronger amplitude on the radial component than on the vertical component. By deconvolving the vertical component signal from the radial component, the effects of the source function and instrument response can be removed, leaving a signal composed of primarily S-wave conversions and reverberations below the seismic station. This time series signal is known as The Receiver Function.

A frequency-domain deconvolution is used to calculate the Fourier transform of the radial receiver function, defined as

$$RF(\omega) = \frac{R(\omega)Z^*(\omega)}{\Phi(\omega)}G(\omega) \quad (1)$$

where ω represents angular frequency, $R(\omega)$ and $Z(\omega)$ are the Fourier transforms of the radial and vertical component respectively and $Z^*(\omega)$ is the complex conjugate of $Z(\omega)$.

$$\Phi(\omega) = \max\{Z(\omega)Z^*(\omega), c \times \max\{(\omega)Z^*(\omega)\}\} \quad (2)$$

and

$$G(\omega) = \xi \exp\left(\frac{-\omega^2}{4a^2}\right) \quad (3)$$

The constant c in (2) represents the water-level (Clayton and Wiggins, 1976), the minimum amplitude allowed in the denominator of (1) for avoiding numerical instabilities in the deconvolution process, and $G(\omega)$ is a low-pass Gaussian filter introduced to simplify the result (Langston, 1979). The constant ξ nor-

malizes the gaussian filter to unit amplitude in the time domain and the constant a determines the width of the gaussian filter. The true receiver function amplitude is estimated by deconvolving the vertical component from itself, using the same water-level parameter in (2) and normalizing the horizontal receiver functions by the maximum amplitude of this vertical component deconvolution (Ammon, 1991).

Inversion method

The receiver-function inversion method consists of a linearized-iterative inversion of a specified waveform by minimizing the misfit residual vector between the observed and modelled receiver function (Ammon et al., 1990). A technique based on the propagator matrix method (Kennet, 1983) is used to compute the synthetic receiver functions for a given velocity model. In theory, the problem may be represented by

$$Gm = dr + Gm_0 \quad (4)$$

where G represents the matrix made up from the partial derivatives of the receiver functions, dr is the residual vector of the receiver-function waveforms, m_0 is the initial velocity model and m is the final velocity model. The inverse problem is solved through a singular-value decomposition of the data kernel G . Details about applying smoothness constraints and calculating the partial derivatives can be found in Ammon et al. (1990) and Randall (1989).

Receiver function computation

In order to compute radial and tangential receiver functions we must isolate the P-waveform from the remaining signal. For the distance ranges used in this study, we use 60 seconds of signal before and 60 seconds after the onset of the P-wave to cover pre-signal noise and most of the S-wave conversion and reverberation beneath the stations. During the source equalization procedure, a water-level of 0.001 was used in most cases, but in few cases 0.0001 and 0.01 was more appropriate. These water-levels were found to be suitable small values that produced acceptable noise levels in the corresponding receiver function (Figure 3). The receiver functions were computed with a Gaussian factor of $a = 2.5$. It has been shown that modelling low frequency receiver functions reduce the potential for biased results caused by scattered energy (Mangino et al., 1993). The selected Gaussian factor

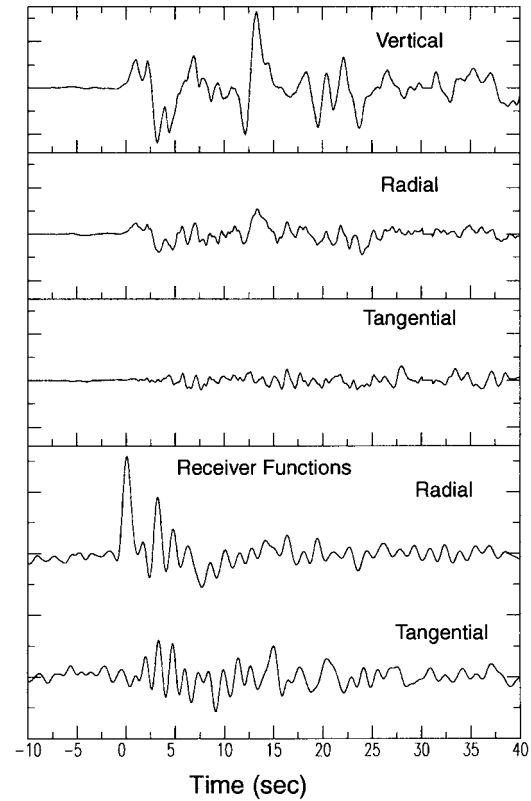


Figure 3. Trace rotated in Z-R-T axis and the corresponding receiver functions of the $M_s = 7.0$ earthquake occurred in Alaska Peninsula on March 20, 1999 recorded by SOR (Soroa) station. The receiver functions were computed with a water-level of 0.001 and a Gaussian factor $a = 2.5$.

still could lead to artefact during the inversion. However, using a lower frequency in the low-pass filter may eliminate the identification of shallow interfaces within the crust. Therefore, the Gaussian factor used was a compromise between reducing the biased result caused by scattered energy and modelling intra crustal interfaces within a thin crust.

To increase the signal to noise ratio, the receiver functions were stacked by similar distances and back-azimuth (Figure 4). The stacking bounds were governed by the available data. The stacks fall in two groups of backazimuth (south and northwest) within a distance bound of about 23° . This wide stacking interval in epicentral distance reduced the identification of scattered energy that should not be quantitatively modelled (Cassidy, 1992). Only two stations (CCC and LMG) have more than one stack. Most of the stations show relatively good quality receiver functions only

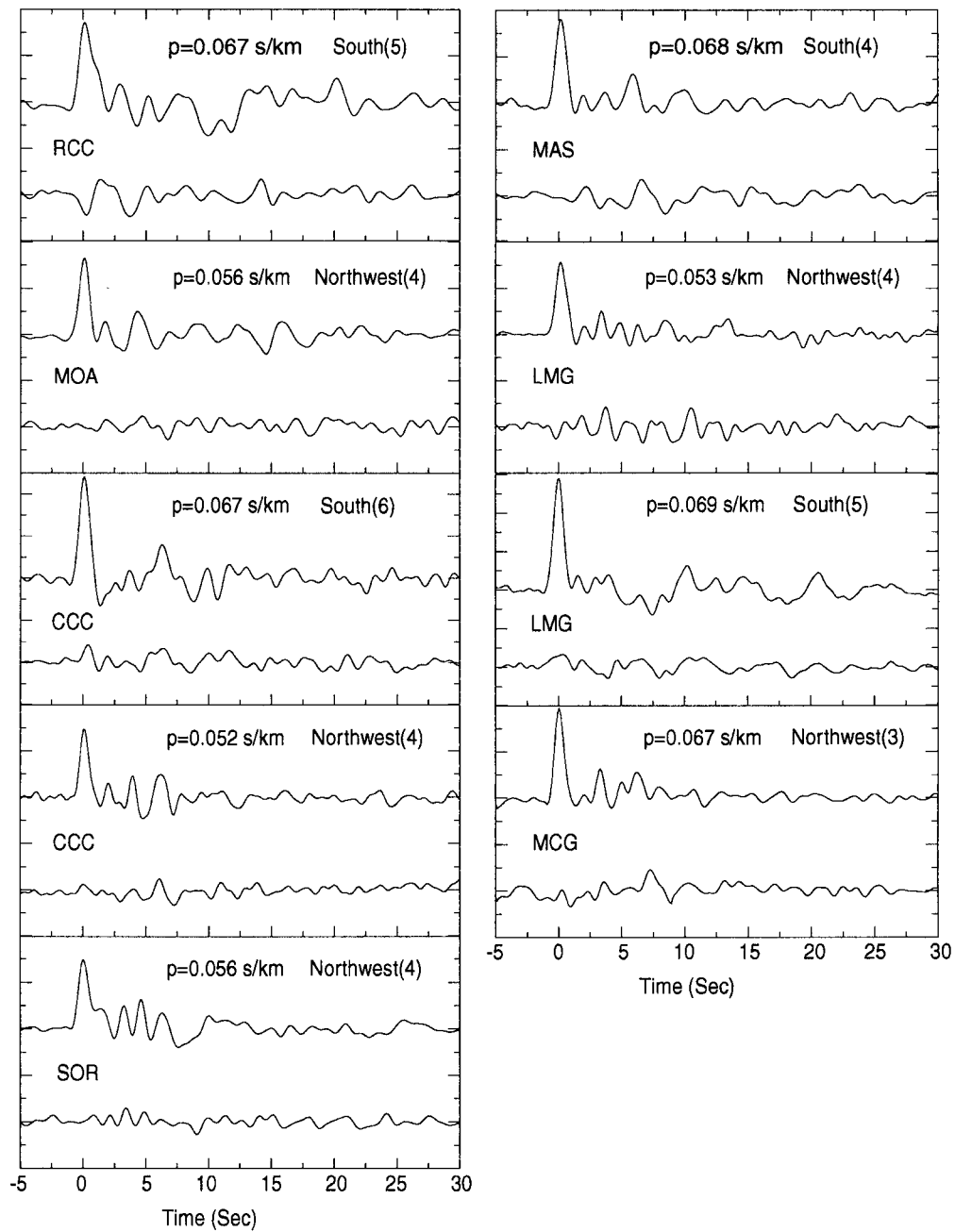


Figure 4. Stacked radial (upper) and tangential (lower) receiver functions for each seismic station. The number of receiver functions used for each stack is shown in parentheses. P indicates the ray parameter.

in one backazimuth direction, which make reliable identification of P-S converted waves at a common vertical velocity discontinuity difficult. The smaller amplitude of the tangential receiver functions relative to the radial receiver functions indicates that the energy appears to be polarized in the vertical-radial plane at most sites. In general, the noise before the direct P arrival is small in most stacks. Individual stacks are described in the next section.

Inversion procedure

Receiver functions are sensitive mainly to shear velocities. Furthermore, to model P-wave velocities a Poisson's ratio has to be assumed. The estimation of Poisson's ratio was based on a Wadati diagram using the SEISAN software (Havskov and Ottemöller, 1999). A V_p/V_s ratio of 1.74 with a standard deviation of 0.07 was obtained. This value is equivalent to a Poisson's ratio of about 0.25. Multiples (i.e. PpPs phases) can be also used to estimate V_p/V_s ratio (Zandt and Ammon, 1995; Zhu and Kanamori, 2000). In this study however, given the limited dataset, it is very difficult to make reliable identification of multiples. Another factor to be estimated is the smoothness trade-off parameter. In this sense, values between 0.1 and 0.9 were tested. A value of 0.2 was found as a good balance between the model roughness and the RMS residual.

It was not possible to use initial models from previous studies because velocities and intra crustal interfaces changes significantly along seismic profiles. Furthermore, the selection of the input models was done by the following procedure. First, a three layer input model was perturbed moving the interfaces up and down within a reasonable range of depths at 1 km intervals. The combination of different layer thicknesses permitted the inversion over 100 input models. The procedure was done for three sets of input velocities, giving a total of 300 models being tested. The objective in this step was to find a good approximation of the first order velocity discontinuities. Afterward, the model with the best fit in terms of model roughness and RMS residual was parameterized with 1 km thick layers and inverted. Then, the obtained output model was randomly perturbed into 40 different starting models using the pseudo-Monte-Carlo technique with a cubic perturbation of 0.75 km/sec (Figure 5). Finally, the output model with the best fit (Figure 6 and Figure 7) was simplified over several inversions

by joining layers with similar velocities. This process ended with a final P-wave velocity model having the minimum possible number of layers and still fitting the observed receiver function relatively well (Figure 8 and Figure 9).

Results

The description of results will be given for Eastern, Central and Western Cuba. The P-wave velocity models and Moho depth for all seismic stations are summarized in Table 4 and Figure 10.

Eastern Cuba

The crustal-mantle interface at RCC (Rio Carpintero) is clearly exhibited in the radial receiver function. The peak of about 2.8 sec correlates with a Ps converted wave at a Moho interface at 18 km (black arrows in Figure 6 and Figure 8). The peak of about 5 sec may be consistent with a multiple PpPs generated at 5 km. The trough shown by the tangential receiver function at about 4 sec suggests that a simple one-dimensional structure does not exist beneath the station.

The radial receiver function at MAS (Maisi) (Figure 6 and Figure 8) indicates an early arrival of about 2 sec, which can be associated with a converted P-S wave at a shallow interface of 13 km (white arrow in Figure 8). The Ps arrival of about 3.5 sec seems to be generated at a Moho interface of 24 km (black arrow in Figure 6 and Figure 8). The late arrival near 6 sec could be associated with a multiple PpPs of the before mentioned shallow interface. However, the tangential receiver function (Figure 4) shows relatively high energy about 6 sec, which suggests that this observed arrival may be contaminated with signal-generated noise (scattered energy) caused by the interaction of the P wave field with lateral velocity variations. Furthermore, the high velocity zone between 3 and 9 km could be an artefact of the inversion process trying to fit the wide peak at 6 sec.

The small amplitude observed in the tangential receiver function at MOA allows for a more confident interpretation in terms of one-dimensional response. The radial receiver function shows a late arrival at about 4 sec suggesting a Moho interface at 29 km (Figure 6 and Figure 8). The peak at about 2 sec may correlate with a velocity discontinuity at 17 km. The tangential receiver function does not reveal any evidence to question the reliability of the significant high-velocity zone introduced by the inversion

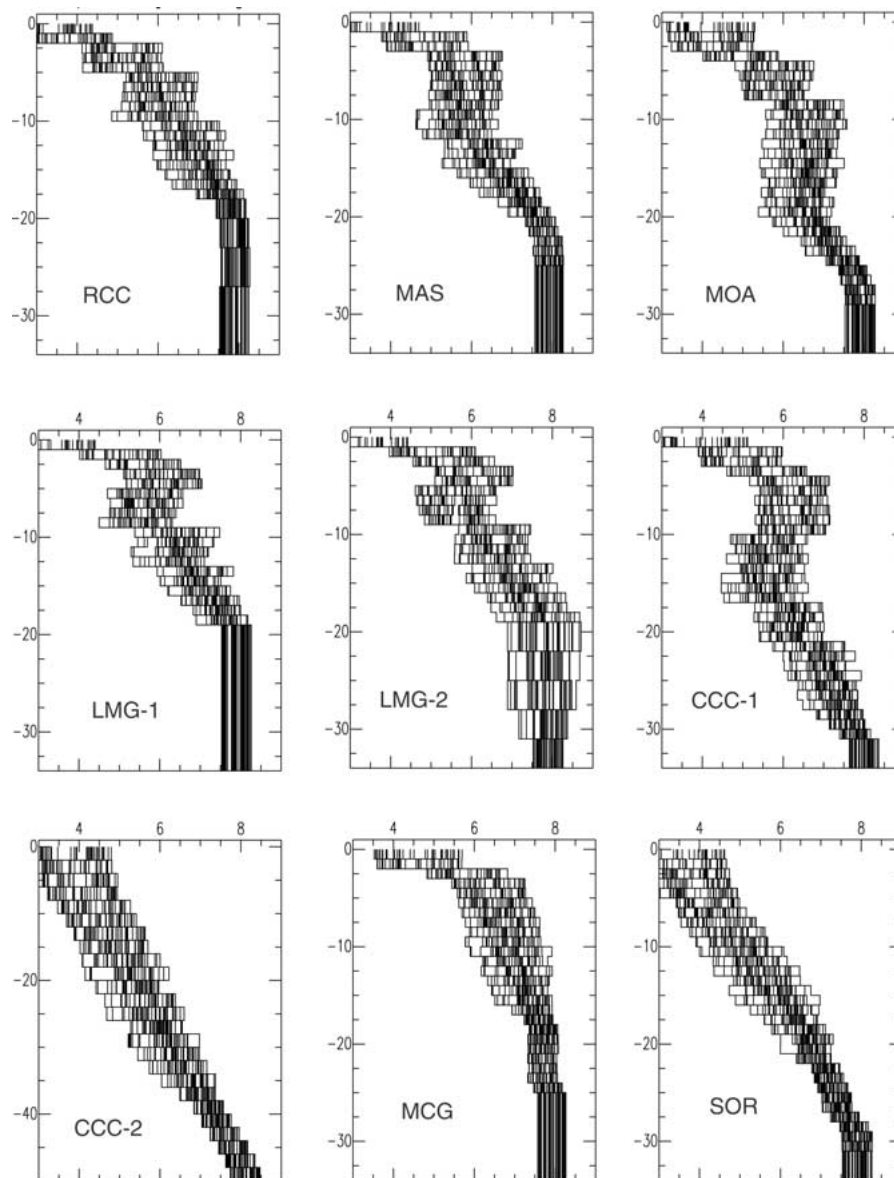


Figure 5. Input models used in the inversion process for each seismic station.

process. Unfortunately, there is no information from seismic refraction profiles near this station to confirm the result.

Figure 4 shows two stacks for LMG (Las Mercedes) station. The radial receiver function for the South stack has P-S converted phases with amplitudes below the signal-generated noise or reverberation and therefore is not a good candidate to model synthetic receiver functions. On the other hand, the radial receiver function for the Northwest stack shows more clear arrivals within the first 7 sec and lower noise

for later arrivals. The Northwest stack was selected to model the structure beneath the station. Two families of input models were used for the inversion (Figure 5). One family (LMG-1) with the last velocity interface at 19 km and another (LMG-2) with the last interface at 31 km. The output models from LMG-1 resulted in synthetic receiver functions having relatively good fit within the first 7 sec. It has an interpreted Moho depth of 19 km (Figure 6). The result from LMG-2 has an interpreted Moho depth of 31 km. In comparison with LMG-1, it fits less well within the first 7 sec but, fits

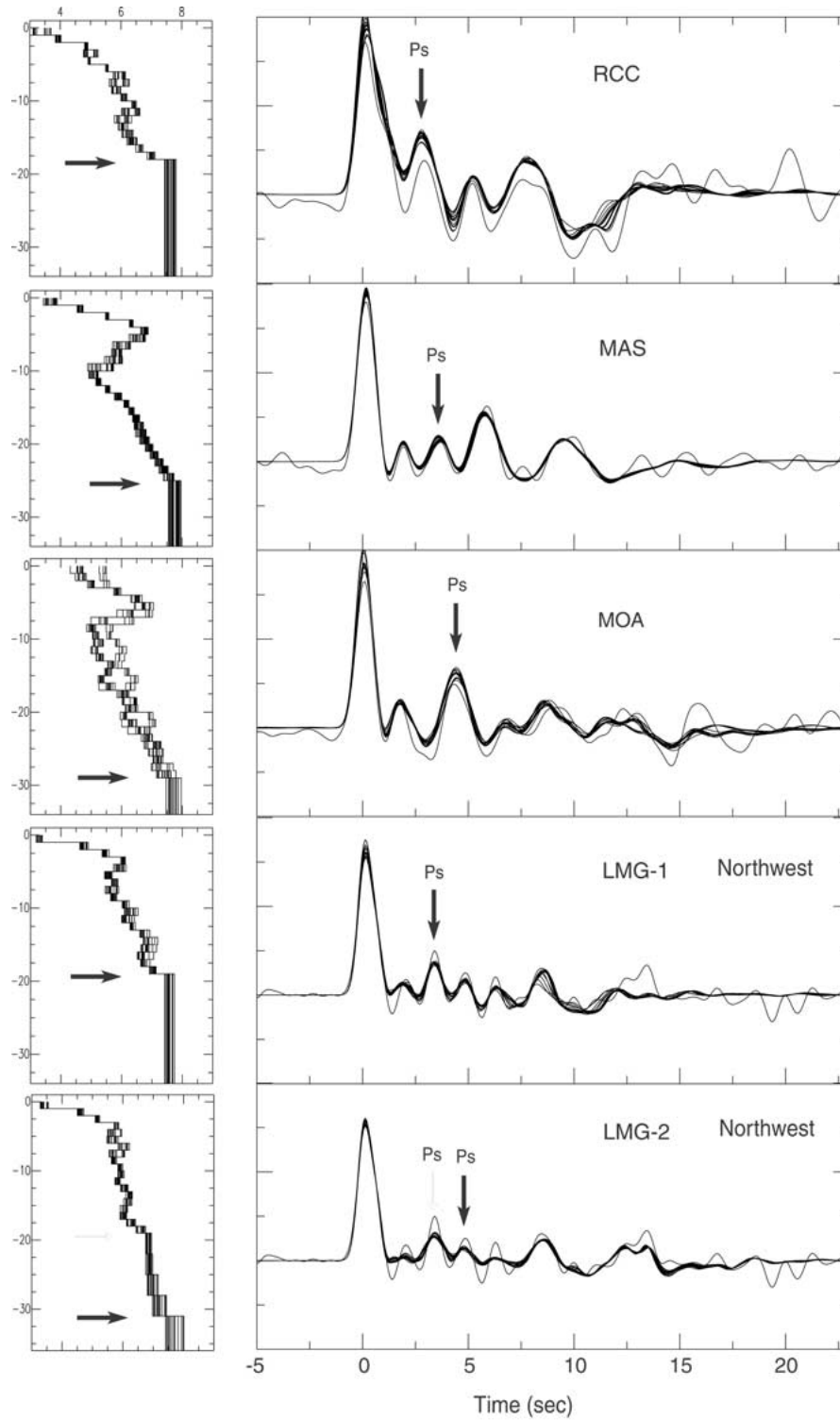


Figure 6. Output models and its corresponding synthetic radial receiver functions of RCC, MAS, MOA and LMG obtained from the inversion. The synthetic radial receiver functions overlap in a solid black line the observed radial receiver function. Black arrows indicate the Moho interface. Only models that fit the observed radial receiver function relatively well are shown.

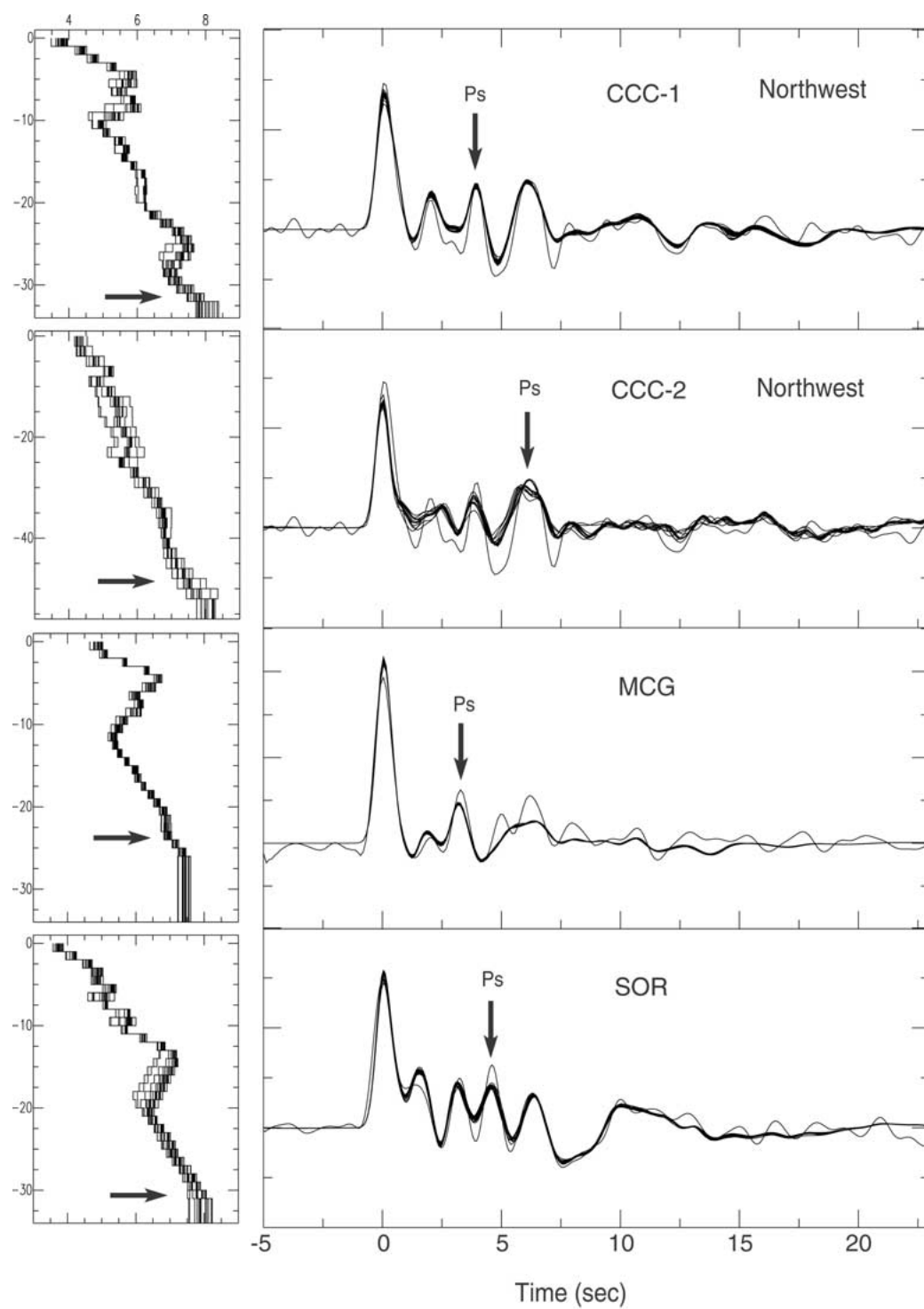


Figure 7. Output models and corresponding synthetic radial receiver functions of CCC, MCG and SOR obtained from the inversion. See caption of Figure 6 for details.

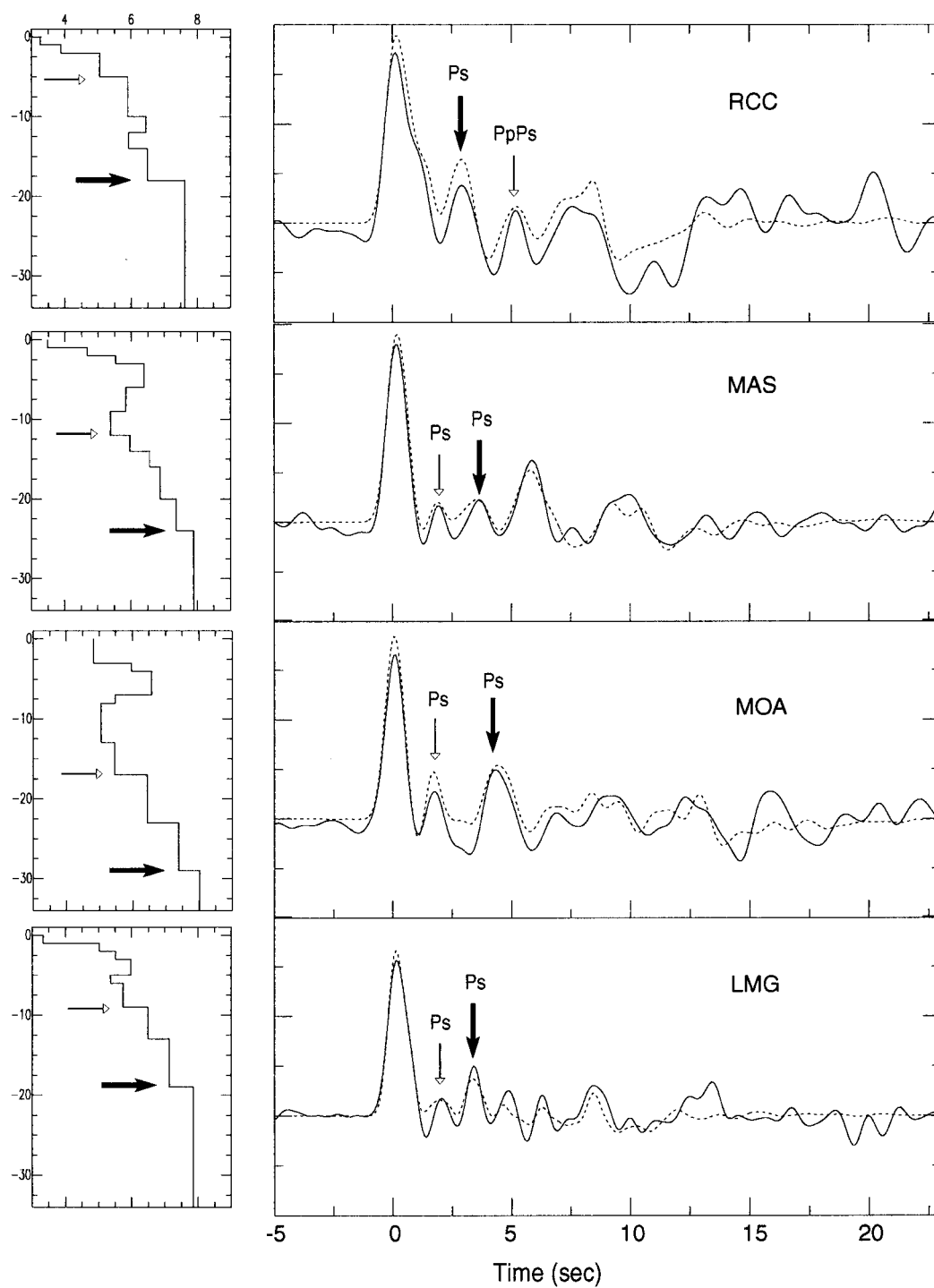


Figure 8. Simplified output model derived from the output models shown in Figure 6 and its corresponding synthetic radial receiver function (dashed line). White arrows indicate interfaces within the crust and black arrows indicate the Moho interface.

better with the peak of later arrivals, for example the peak of about 13 sec. This later arrival may represent scattered energy, which should not be quantitatively modelled. LMG-1 shows more confident results in terms of fitting the observations and conforms with previous knowledge of crustal thickness in the area. These two inversions were done to show why most of the input models shown in Figure 5 have the last interface relatively close to the deepest major interface that we want to determine, which in this case is the Moho interface. Using input models with interfaces much more deeper than the probable Moho depth could increase the risk of misinterpretations. Note that the last interface was estimated in an earlier step.

The simplified LMG-1 model is shown in Figure 8. Two Ps arrivals can be identified. The earlier peak at about 2 sec is consistent with a Ps converted wave at 9 km and the next peak at about 3 sec is interpreted as a Ps phase generated at a Moho interface. The tangential receiver function shows relatively high amplitude, which reduces the confidence of the interpretation since it is based only in a simple one-dimensional response. An evidence of the complexity of the structure beneath the station is the fact that there is not a good coherence of Ps phases between the South and Northwest stacks.

CCC (Cascorro) is the station with most available data. Figure 4 shows two stacks for this station, the South and the Northwest. The radial receiver function for the Northwest stack is the best candidate for modelling synthetic receiver functions. It has clear arrivals within the first 7 sec and low signal-generated noise. Both stacks have common peaks of about 4 and 6 sec respectively. The peak at about 4 sec can be considered as a Ps generated wave. On the other hand, the later arrival may be analyzed as one of three possibilities: (1) a multiple PpPs, (2) a Ps phase at deep interface and (3) scattered energy. The last possibility can be rejected because scattered energy should not appear at a similar time for different azimuths. Between the first two possibilities, the first one gives a result more consistent with previous seismic refraction studies in the area and seems to be the more reasonable solution. Nevertheless, both solutions are shown in Figure 7 and Figure 9. The first solution (CCC-1) has a very good fit and suggests a Moho interface at 31 km, which correlates with the peak at about 4 sec. The earlier peak at about 2 sec seems to be a Ps phase generated at 13 km. The peak at 6 sec may be associated with a PpPs phase at 13 km. Note that the relative amplitude of the multiple in comparison to the am-

plitude of the Ps phase depends on the incident angle. At near vertical and grazing P-wave incidence there is no reflected SV wave. However, there is a wide range of incidence angles (50° – 80°) over which most of the energy is reflected as SV (Stein, 1991). For example, forward modelling indicates that a receiver function generated with a simple 10 km thick one-layer model of 5.7 km/sec at the surface and 7.6 at the half space and a ray parameter of 0.04 s/km shows a multiple with a larger amplitude than the Ps phase. On the other hand using a ray parameter of 0.08 s/km, which generates steeper incidence, a multiple with lower amplitude than the Ps phase is exhibited.

The second solution (CCC-2) poorly fits the earlier arrivals. It suggests a deep interface of about 48 km. This interface could be interpreted either as the Moho or a discontinuity in the mantle. The Moho interpretation seems unreasonable because it is unlikely to have such a big change in the crustal thickness within such a small area. Although there is not enough argument to support a unique solution for the structure beneath this station, the first possibility (CCC-1) is proposed as a more reasonable solution, but it does not mean that the possible deep interface at 48 km must be rejected. Both, the PpPs at a shallower interface and the Ps at a deeper interface will be seen in a single peak if they have similar arrival times.

Central Cuba

The receiver function analysis for this part of the country was limited by the few earthquakes recorded by MCG (Manicaragua) station. The peak of about 3.5 sec can be associated with a Ps phase generated at a Moho interface of about 24 km (Figure 7 and Figure 8). The low velocity zone between 9 and 13 km is introduced to fit the trough at about 4 sec. The peaks near 6 sec could be a multiple but it is not well resolved by the inversion. The tangential receiver function shows relatively high energy at about 7.5 sec but, since it occurs at a different time, it is unlikely to correlate the observed peak at 6 sec in the radial receiver function with scattering.

Western Cuba

The Ps phase at about 4.3 sec in the receiver functions of SOR (Soroa) suggests a Moho depth of about 30 km (Figure 7). The simplified model (Figure 9) reduced the Moho depth to 27 km. This model is more reliable given its simple layering and keeps almost the same fit as the model shown in Figure 7. The earlier arrival at

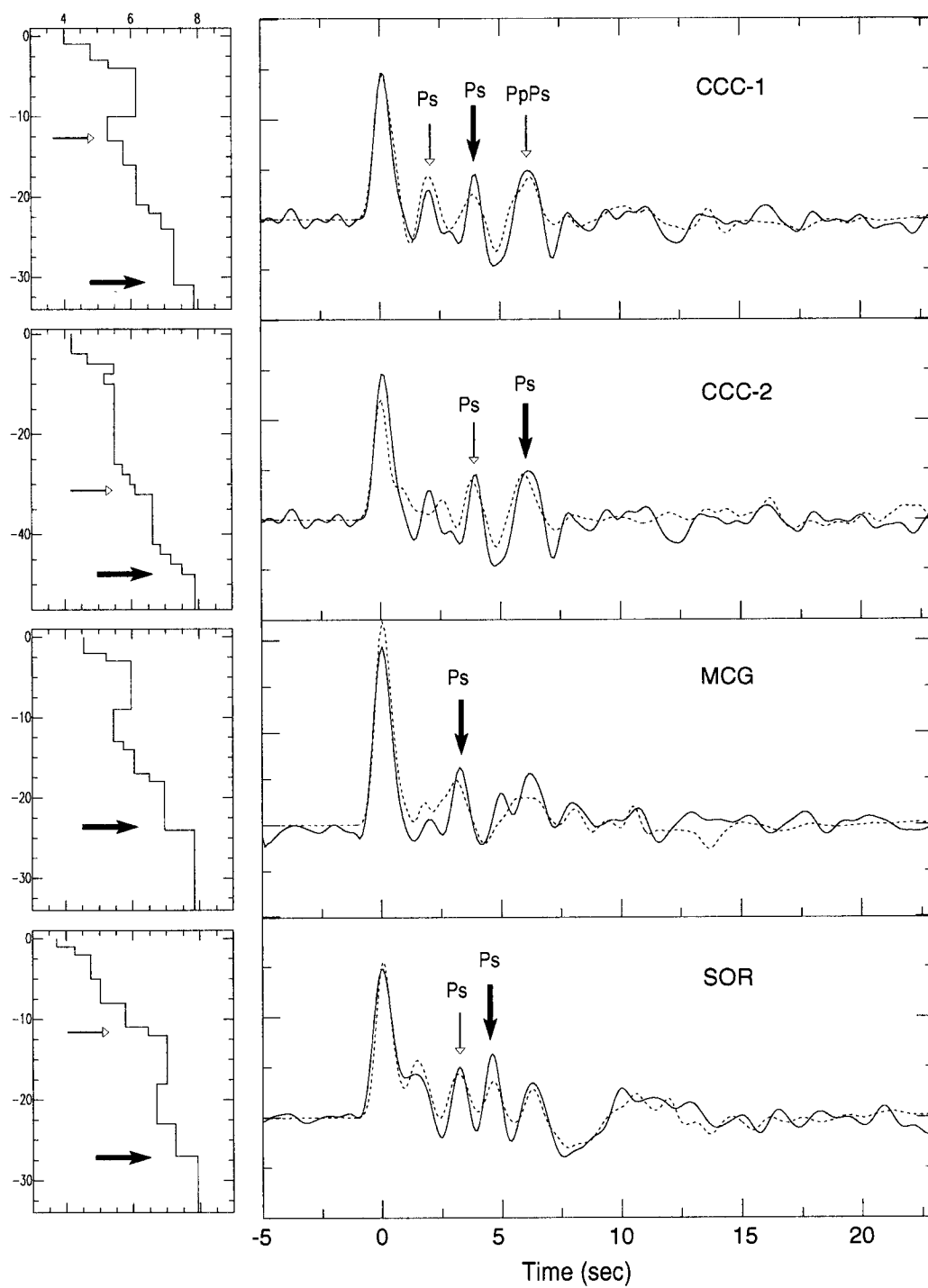


Figure 9. Simplified output model derived from the output models shown in Figure 7 and its corresponding synthetic radial receiver function (dashed line). White arrows indicate interfaces within the crust and black arrows indicate the Moho interface.

Table 3. Relation of crustal thickness at seismic stations derived from different studies. Question mark (?) is indicating probable thickness given distance from seismic cross sections shown in Figure 1

Stations	Shcherbakova et al., 1977, 1978	Bovenko et al., 1980, 1982	Bush and Shcherbakova, 1986	This study
MAS	–	–	–	24 km
MOA	–	–	–	29 km
RCC	–	18 km (?)	–	18 km
LMG	–	21 km (?)	17–24 km (?)	19 km
CAS	–	32 km	35 km	31 km
MCG	30 km	–	17–24 km (?)	24 km
SOR	30 km	–	30 km (?)	27 km

Table 4. P-wave velocity models obtained in this study. P-wave velocity (Vp) in km/sec and depth in km

Stations/ Layers	RCC (Vp/depht)	MAS	MOA	LMG	CCC	MCG	SOR
1	3.26/0	3.48/0	4.84/0	3.32/0	4.00/0	4.55/0	3.73/0
2	3.88/1	4.67/1	5.98/3	5.02/1	4.80/1	5.22/2	4.26/1
3	5.05/2	5.53/2	6.58/4	5.51/2	5.33/3	5.97/3	4.73/2
4	5.90/5	6.40/3	5.47/7	5.98/3	6.15/4	5.43/9	5.02/5
5	6.45/10	5.85/6	5.05/8	5.36/5	5.30/10	5.73/13	5.77/8
6	5.93/12	5.37/9	5.46/13	5.74/6	5.76/13	6.05/14	6.45/11
7	6.50/14	5.97/12	6.44/17	6.48/9	6.15/16	6.49/17	7.02/12
8	7.62/18	6.57/14	7.39/23	7.20/13	6.53/21	6.95/18	6.70/18
9		6.89/16	8.01/29	7.85/19	6.89/22	7.84/24	7.26/23
10		7.36/20			7.27/24		7.93/27
11		7.89/24			7.86/31		

about 3 sec might be consistent with a Ps phase generated at 12 km. Note that the delay for these phases is larger in comparison with other stations due to the low velocity of the first 12 km thick layer. The low velocity zone between 18 and 23 km is introduced to fit the trough at 7.5 sec. The tangential receiver function (Figure 4) shows small scattering at this site, which makes the interpretation in terms of a one-dimensional response more confident.

Discussion

In eastern Cuba, the crustal thickness obtained in this study is consistent with previous results at most sites (Table 3 and Figure 10). At two stations (MAS and MOA), it was not possible to compare with seismic profiles. According to Otero et al. (1998), MOA and

MAS are located on oceanic crust with thickness lower than 20 km (Figure 1). However, there is no seismic profile close to this area to verify this. Their result is based on extrapolation. The crust at MOA seems to be much thicker than oceanic-crust type. It is located on the north coast, near to the contact zone between the Bahama platform and the Cuban block (Moreno, 2002). There is a compressional deformation along this contact zone (Moreno, 2002), which could generate crustal thickening in this area. RCC seems to be the station with the thinnest crust in this area. Two of the seismic profiles (XI and XII, Figure 1) show evidence of gradual thinning of the crust in a southward direction, characterizing the extreme southern block with oceanic crust (Bush and Shcherbakova, 1986). LMG is located close to one of these profiles (Profile XI), where Bush and Shcherbakova (1986) found deep faults causing significant changes in the crustal thick-

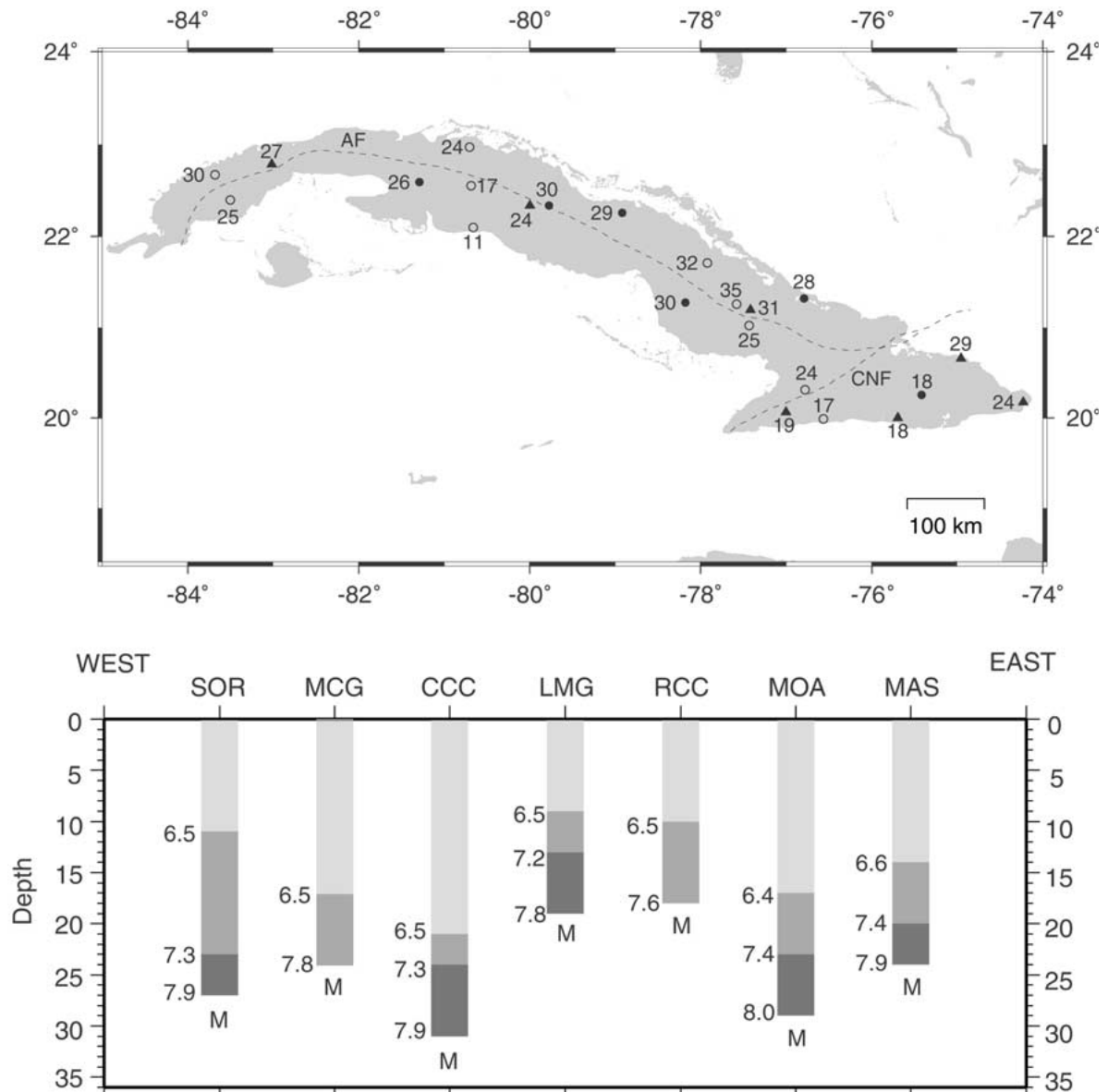


Figure 10. Upper map: Crustal thickness at different sites in Cuba. Triangle – Moho depth at seismic stations derived in this study. Open circle – Moho depth derived from joint interpretation of gravity and seismic refraction data (Bush and Shcherbakova, 1986). Closed circle – Moho depth derived from seismic refraction methods (Shcherbakova et al., 1977, 1978; Bovenko et al., 1980, 1982). Dashed lines as Figure 2. Lower graph: Major discontinuities revealed from receiver function inversions at each station.

ness and lateral velocity variation. Evidence of the scattered energy generated by this anisotropic medium is shown in the LMG-Northwest tangential receiver function (Figure 4). The site with most available information is CAS having a seismic profile very close (XI, Figure 1). This station seems to be located on the thickest crust in the area and probably the thickest crust in Cuba.

Previous studies have shown disagreements in the crustal thickness in central Cuba. Shcherbakova et al. (1977, 1978) suggested a crustal thickness between 28–32 km along Profile V (Figure 1). However, Bush and Shcherbakova (1986) claim that the central Cuba seems to be the area with the thinnest crust ranging from 24 km (north) to 11 km (south) along Profile V (Figure 1 and Figure 10). They pointed out that the deep interfaces at 29–32 km found by Shcherb-

akova et al. (1977,1978) was erroneously interpreted and was accounted for by processing error. The result in this study is consistent with the interpretation made by Otero et al. (1998), which classified this area as a thin transitional crust (Figure 1). Western Cuba with only one site (SOR) seems to be in good agreement with previous studies.

Upper-mantle P-wave velocities have not been well constrained by previous studies. In most cases 8.1 km/sec has been assumed. The receiver function inversion suggests a velocity between 7.6 and 8.0 km/sec in eastern Cuba, 7.8 and 7.9 km/sec for the central and western part of the country, respectively. Figure 10 (lower graph) shows an interpretation of the major discontinuities beneath the seismic stations. The interface with 6.5 km/sec is interpreted as the top of the 'basalt' layer. Before the mantle interface, a discontinuity with velocities between 7.3 and 7.4 km/sec is revealed at most stations. This could be associated with a top of the crust-mantle transition zone.

Low velocity zones are commonly obtained in receiver function analysis. The potential to introduce this feature increases when modelling high frequency receiver functions because of the biasing effect of scattered energy generated by lateral heterogeneity at higher frequencies. In this study there is a potential for the biasing effect because the low-pass filter used is not low enough to eliminate the effect of the high frequency scattered energy. Therefore, the low velocity zones obtained at several sites could be artefacts introduced by the inversion process.

In general we can conclude that the results obtained in this study suggest the existence of both oceanic and continental crust in Cuba. The oceanic crust is found in the extreme southern coast, whereas the north coast seems to be characterized by a continental crust. This pattern has been shown by previous studies (Bush and Shcherbakova, 1986), which indicates that this significant change in the crust occurs across the southern boundary of the Bahama platform and the Cuban block.

Acknowledgements

The author is grateful to Lars Ottemöller for his useful advise and review of the manuscript. Charles Ammon's programs and guide on receiver function were the basis of this study. Thanks also to Kuvvet Atakan and Jens Havskov for their comments and suggestion during the review of this paper. The staff at the

Cuban Seismological Service provided support in obtaining the data. Margaret Grandison improved the overall quality of the manuscript. The comment of two anonymous referees greatly improved this work.

References

- Ammon, C.J., Randall, G.E. and Zandt, G., 1990, On the nonuniqueness of receiver function inversions, *J. Geophys. Res.* **95**, 15303–15318.
- Ammon, C.J., 1991, The isolation of receiver effects from teleseismic P wave fronts, *Bull. Seism. Soc. Am.* **81**, 2504–2510.
- Bovenko, V.G., Shcherbakova, B.E. and Hernández, H., 1980,1982, Novyye geofizicheskiye dannyye o glubinnour stroyenii vostochnoy kuby (New geophysical data on the deep structure of eastern Cuba), *Sovetskaya Geologiya* **9**, 101–109; translation in *International Geology Review* **24**, 1155–1162.
- Bush, V.A. and Shcherbakova I.N., 1986, New Data on the Deep Tectonics of Cuba, *Geotectonics* **20**, 192–203.
- Case, J.E., MacDonald, W.D. and Fox, P.J., 1990, Caribbean crustal provinces; Seismic and gravity evidence, In: Dengo, G. and Case, J.E. (eds), *The Geology of North America, The Caribbean Region*, Vol. **H**, pp. 15–36, Geological Society of America, Boulder, Colorado.
- Cassidy, J.F., 1992, Numerical experiments in broadband receiver function analysis, *Bull. Seism. Soc. Am.* **82**, 1453–1474.
- Clayton, R.W. and Wiggins, R.A., 1976, Source shape estimation and deconvolution of teleseismic body waves, *Geophys. J. R. astr. Soc.* **47**, 151–177.
- Draper, G. and Barros, J.A., 1994, Cuba (chapter 4), In: *Caribbean Geology: An Introduction*, U.W.I. Publishers' Association, Kingston, pp. 65–85.
- Goldstein, P., 1999, *SAC User's Manual*, Lawrence Livermore Laboratory, University of California.
- Havskov J. and Ottemöller, L., 1999, *SEISAN: The Earthquake Analysis Software*, Version 7.0, Institute of Solid Earth Physics, University of Bergen, Norway, 226 pp.
- Kennett, B.L., 1983, *Seismic Wave Propagation in Stratified Media*, Cambridge University Press, Cambridge, England.
- Langston, C.A., 1979, Structure under Mount Rainier, Washington, inferred from teleseismic body waves, *J. Geophys. Res.* **84**, 4749–4762.
- Makarov, V.I., 1986, The Neotectonics of Eastern Cuba. Part One. General Description. Northern and Central Districts, *Geotectonics* **20**, 515–523.
- Mangino, S.G., Zandt G. and Ammon, C.J., 1993, The receiver structure beneath Mina, Nevada, *Bull. Seism. Soc. Am.* **83**, 542–560.
- Moreno, B., 2002, The new Cuban Seismograph Network, *Seism. Res. Lett.* **73**, 505–518.
- Otero, R., Prol, J.L., Tenreyro, R. and Arriaza, G.L., 1998, Características de la corteza terrestre de Cuba y su plataforma marina (Characteristics of the Earth's crust in Cuba and its marine platform), *Mineria y Geología* **15**, 31–35.
- Pardo, G., 1975, Geology of Cuba (chapter 13), In: Nairn, A.E.M. and Stehli, F.G. (eds), *The Ocean Basins and Margins*, Vol. **3**, pp. 553–615, Plenum Publishing, New York.
- Pushcharovskiy, Y.M., 1979, The tectonics and geodynamics of the Caribbean region, *Tektonicheskoye razvitiye zemnoy kory i razlomny* (Tectonic Evolution of the Earth's Crust and Faults), Moscow, Nauka, pp. 124–132.

- Randall, G.E., 1989, Efficient calculation of differential seismograms for lithospheric receiver functions, *Geophys. J. Int.* **99**, 469–481.
- Shcherbakova, B.E., Bovenko, V.G. and Hernández, H., 1977, 1978, Stroyeniye zemnoy kory Zapadnoy Kuby (Crustal structure in West Cuba), *Sovetskaya Geologiya* **8**, 138–143; translation in *International Geology Review* **20**, 1125–1130.
- Soloviev, O.N., Skidan, S.A., Skidan, I.K., Pankratov, A.P. and Judoley, C.M., 1964, Comentarios sobre el mapa gravimétrico de la Isla de Cuba. Cuba, La Habana, Ministerio de Industrias, *Revista Tecnológica* **2**, 8–19.
- Stein, S., 1991, *Introduction to Seismology, Earthquakes and Earth Structure*, Department of Geological Sciences, Northwestern University, 553 pp.
- Zandt, G. and Ammon, C.J., 1995, Continental-crust composition constrained by measurements of crustal Poissons ratio, *Nature* **374**, 152–154.
- Zhu, L. and Kanamori, H., 2000, Moho depth variation in southern California from teleseismic receiver functions, *J. Geophys. Res.* **105**, 2969–2980.

